

## Article

# Synthesis, Thermal and Optical Characterizations of New Lateral Organic Systems

Laila Ahmed. Al-Mutabagani <sup>1</sup>, Latifah A. Alshabanah <sup>1</sup>, Sobhi M. Gomha <sup>2,3</sup> and Hoda A. Ahmed <sup>2,4,\*</sup> 

- <sup>1</sup> Department of Chemistry, College of Science, Princess Nourah bint Abdulrahman University, Riyadh 11671, Saudi Arabia; laalmutbagani@pnu.edu.sa (L.A.A.-M.); laalsabanah@pnu.edu.sa (L.A.A.)  
<sup>2</sup> Department of Chemistry, Faculty of Science, Cairo University, Cairo 12613, Egypt; sm.gomha@iu.edu.sa  
<sup>3</sup> Chemistry Department, Faculty of Science, Islamic University in Almadinah Almonawara, Almadinah Almonawara 42351, Saudi Arabia  
<sup>4</sup> Chemistry Department, College of Sciences, Yanbu, Taibah University, Yanbu 30799, Saudi Arabia  
\* Correspondence: ahoda@sci.cu.edu.eg

**Abstract:** New laterally OCH<sub>3</sub>-substituted optical organic Schiff base/ester series, namely 4-(4-(hexyloxyphenyl)iminomethyl)-3-methoxyphenyl 4-alkoxybenzoates, were prepared and characterized with different thermal, mesomorphic, and photoactive techniques. The prepared group constitutes five homologues that differ from each other in the number of carbons in the terminal alkoxy chain (*n*), which varies between *n* = 6, 8, 10, 12, and 16 carbons. The laterally protruded methoxy group is attached to the central benzene ring that makes an angle of 120° with the molecular long axis. Molecular structures of all newly prepared homologues were fully elucidated via FT-IR, <sup>1</sup>H and <sup>13</sup>C NMR spectroscopy. Mesomorphic transitions were determined via differential scanning calorimetry (DSC) and the phases identified by polarized optical microscopy (POM). Independent of the length of the terminal alkoxy chain attached to phenyl ester ring, only a monomorphic nematic (N) phase was observed for all the synthesized compounds. A comparative study was made between the present lateral methoxy-substituted homologues and their corresponding laterally-neat analogues. The results revealed that, depending on the length of the alkoxy chain and the presence or absence of the lateral methoxy group, different mesophases with different thermal stability and temperature ranges were observed. Finally, UV-vis spectra showed that the present nematogenic series possess photoactive properties that are of importance for many applications.

**Keywords:** Schiff base/ester; optical properties; thermal parameters; mesophase stability; photo-physical



**Citation:** Al-Mutabagani, L.A.; Alshabanah, L.A.; Gomha, S.M.; Ahmed, H.A. Synthesis, Thermal and Optical Characterizations of New Lateral Organic Systems. *Crystals* **2021**, *11*, 551. <https://doi.org/10.3390/cryst11050551>

Academic Editor: Antonio Martins Figueiredo Neto

Received: 17 April 2021  
Accepted: 13 May 2021  
Published: 15 May 2021

**Publisher's Note:** MDPI stays neutral with regard to jurisdictional claims in published maps and institutional affiliations.



**Copyright:** © 2021 by the authors. Licensee MDPI, Basel, Switzerland. This article is an open access article distributed under the terms and conditions of the Creative Commons Attribution (CC BY) license (<https://creativecommons.org/licenses/by/4.0/>).

## 1. Introduction

Optical and mesomorphic characteristics of organic compounds are mainly dependent on their geometries, in which slight modification in the structure is associated with a considerable change in their mesophase behavior. Large numbers of calamitic thermotropic liquid crystalline materials, with rigid cores containing two or more aromatic rings and terminal flexible chains, have been prepared [1–3]. Many of these investigations were based on the Schiff bases linkage [4–7]. It is worth mentioning that the first room-temperature nematogenic material, namely 4-methoxybenzylidene-4'-butylaniline (MBBA), was investigated by Kelker et al. [8].

The incorporation of a high polar, small size lateral group to the main architecture of the molecule influences the physical or thermal properties of the forming mesomorphic material, such as melting temperature, phase transition temperature, morphology, dielectric anisotropy and dipole moment [9–13]. In such cases, the intermolecular separation increases by the addition of the lateral substituent, which broadens the molecular core, leading to the depression of the lateral-interactions [14–16]. Furthermore, as the molecule width increases, the stability of both the smectic and nematic phases will be

reduced [17]. The small size of the lateral substituent enables its incorporation within the mesomorphic geometrics without being sterically disrupted and, consequently, their mesophases are still observed. It was reported that the mesophase type, stability and range were affected by the protrusion of a lateral-fused ring in the central core of mesogenic part of the molecule [18]. In another work [19], disruption of the mesophase was observed in a laterally nitro substituted series due to the increase of the molecular width, which affected its lateral intermolecular interactions. In addition, the high dipole moment and steric hindrance of the NO<sub>2</sub> group disrupted their mesomorphic properties.

On the other hand, the length of the terminal flexible chain plays a significant role in mesomorphic behavior, enhancing the twist-bend nematic and heliconical phases [20]. It has also been reported that the lateral or terminal polar group processes an impact effect on the mesomorphic properties of a large number of Schiff bases/ester systems [21].

The growing interest of optical organic materials in the last few decades is because of their photo-physical properties [22] that lead to industrial applications, such as laser dyes and fluorescent brighteners [23]. Due to their reasonable thermal stabilities, they have been widely used in photonic and electronic applications, such as solar cells, charge-transfer agents and non-linear optical (NLO) materials. Most of them are based on chromophores and constitute one of the highest types of fluorescence sensors [24–26], which accounts for its exponentially increased application, such as fluorescent probes [27,28]; they are also broadly used in organic light-emitting diodes [29]. Moreover, the thermal property causes the nematogenic materials to flow and their optical responses, activated by small temperature changes, can be used in sensing and photonics applications [30]. It was found that this effect had essential ramifications for the nematic phases as the optical properties of thermally induced geometrical changes [30].

Recently, in further structure–property relationship studies of calamitic liquid crystals, the molecular biaxiality of the rode-like molecules was increased by introducing a lateral methoxy (–OCH<sub>3</sub>) group within the molecular skeleton. From this point of view, the first goal of our present work is to synthesize new geometrical structure of laterally substituted three rings Schiff base derivatives, bearing terminal alkoxy chains with different lengths (*n*), namely, 4-(4-(hexyloxyphenyl)iminomethyl)-3-methoxyphenyl 4-alkoxybenzoates (Figure 1). The lateral OCH<sub>3</sub> group is attached to the middle ring. The second goal is to investigate their optical, mesomorphic, and photophysical behaviors as well as to study the impact of the terminal flexible alkoxy chain on the mesomorphic properties of prepared compounds. Finally, a comparison will be made between the present laterally substituted derivatives and their previously reported three rings Schiff base analogues in order to investigate the effect of the introduction of lateral substituent on their mesophase behavior.

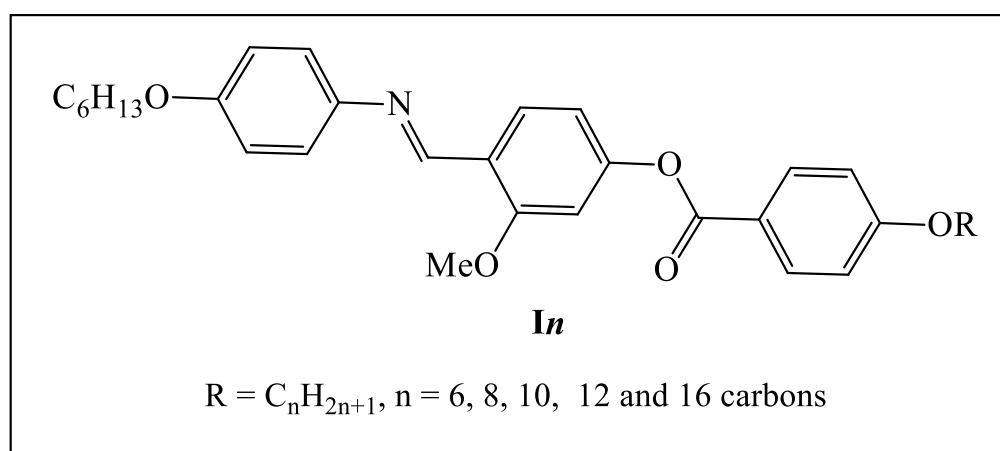
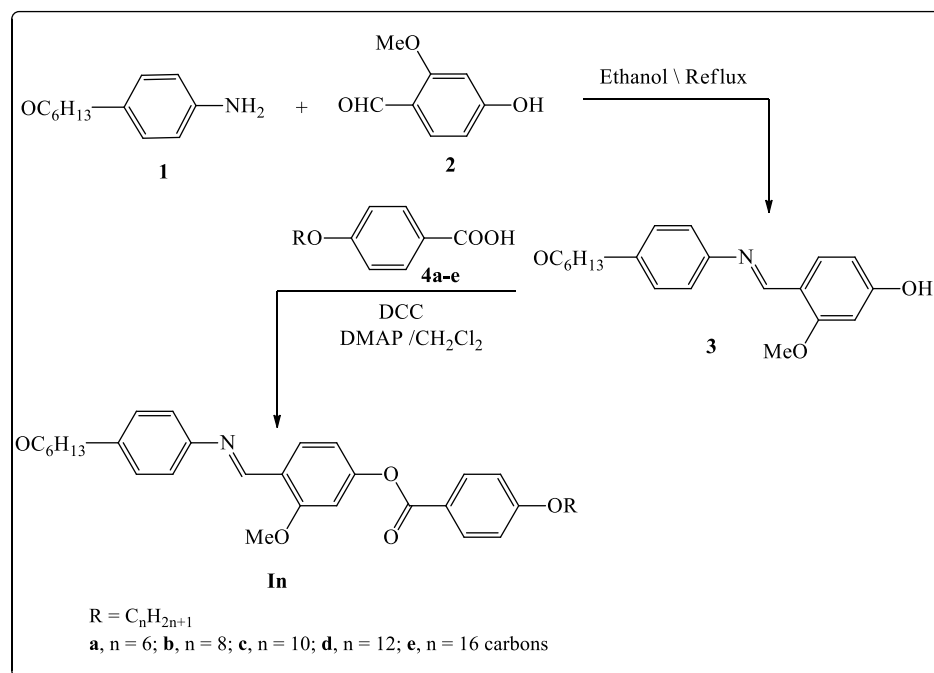


**Figure 1.** Chemical structure of 4-(4-(hexyloxyphenyl)iminomethyl)-3-methoxyphenyl 4-alkoxybenzoates, **In**.

## 2. Experimental

### Synthesis

Schiff base and hydrazone derivatives are well known as valuable intermediates in the synthesis of many organic compounds that are used in many applications [31–39]. A series of new laterally methoxy Schiff base derivatives **3** and **In** were formed as the following shown in Scheme 1:



**Scheme 1.** Synthesis of 4-(4-(hexyloxyphenyl)iminomethyl)-3-methoxyphenyl 4-alkoxybenzoates, **In**.

Synthetic method is attached in the supplementary data. The melting points and IR data were determined for the prepared imine **3**: Yield: 90.1%; mp 101.1 °C, FTIR ( $\nu$ ,  $\text{cm}^{-1}$ ): 3400 (OH), 2928, 2832 ( $\text{CH}_2$  stretching), 1733 (C=O), 1609 (C=N), 1566 (C=C), 1466 (C-O<sub>Asym</sub>), 1251 (C-O<sub>Sym</sub>). <sup>1</sup>H-NMR (400 MHz,  $\text{CDCl}_3$ ):  $\delta$ /ppm: 0.85–0.90 (t, 3H,  $\text{CH}_3(\text{CH}_2)_3\text{CH}_2\text{CH}_2\text{O}-$ ), 1.29–1.31 (m, 6H,  $\text{CH}_3(\text{CH}_2)_3\text{CH}_2\text{CH}_2\text{O}-$ ), 1.71–1.78 (q, 2H,  $\text{CH}_3(\text{CH}_2)_3\text{CH}_2\text{CH}_2\text{O}-$ ), 3.72 (s, 1H, OH), 3.93 (s, 3H,  $\text{OCH}_3$ ), 4.08 (t, 2H,  $\text{CH}_3(\text{CH}_2)_3\text{CH}_2\text{CH}_2\text{O}-$ ), 6.79 (d, 2H, Ar-H), 6.89 (d, 2H, Ar-H), 7.01 (d, 2H, Ar-H), 7.24 (s, 1H, Ar-H), 7.38–7.40 (m, 3H, Ar-H), 7.84 (d, 2H, Ar-H), 9.76 (s, 1H, CH=N). Anal. Calcd. for  $\text{C}_{20}\text{H}_{25}\text{NO}_3$  (327.42): C, 73.37; H, 7.70; N, 4.28. Found: C, 73.21; H, 7.59; N, 4.13%.

### General Procedure for Synthesis of 4-(4-(hexyloxyphenyl)iminomethyl)-3-Methoxyphenyl 4-Alkoxybenzoates

Synthetic method is attached in the supplementary data. The physical data of products **In** are listed below:

#### 4-(4-(Hexyloxyphenyl)iminomethyl)-3-methoxyphenyl 4-hexyloxybenzoate (**I6**).

Yield: 88.2%; mp 114–116 °C, FTIR ( $\nu$ ,  $\text{cm}^{-1}$ ): 2929, 2869 ( $\text{CH}_2$  stretching), 1735 (C=O), 1612 (C=N), 1573 (C=C), 1458 (C-O<sub>Asym</sub>), 1260 (C-O<sub>Sym</sub>). <sup>1</sup>H-NMR (400 MHz,  $\text{CDCl}_3$ ):  $\delta$ /ppm: 0.86–0.97 (m, 6H,  $2 \times \text{CH}_3(\text{CH}_2)_3\text{CH}_2\text{CH}_2\text{O}-$ ), 1.23–1.33 (m, 12H,  $2 \times \text{CH}_3(\text{CH}_2)_3\text{CH}_2\text{CH}_2\text{O}-$ ), 1.78–1.80 (m, 4H,  $2 \times \text{CH}_3(\text{CH}_2)_3\text{CH}_2\text{CH}_2\text{O}-$ ), 3.88 (s, 3H,  $\text{OCH}_3$ ), 4.01–4.05 (m, 4H,  $2 \times \text{CH}_3(\text{CH}_2)_3\text{CH}_2\text{CH}_2\text{O}-$ ), 6.81 (s, 1H, Ar-H), 6.94–6.97 (m, 3H, Ar-H), 7.31–7.33 (d, 2H, Ar-H), 7.51 (d, 2H, Ar-H), 8.12–8.14 (m, 3H, Ar-H), 9.95 (s, 1H, CH=N). <sup>13</sup>C-NMR (100 MHz,  $\text{CDCl}_3$ ):  $\delta$ /ppm: 14.0 (2 $\text{CH}_3$ ), 18.3, 22.5, 22.6, 25.6, 29.0, 29.6, 31.5, 31.9 (8 $\text{CH}_2$ ), 56.1 ( $\text{OCH}_3$ ), 68.3, 68.4 (2 $\text{CH}_2\text{-O}$ ), 109.5, 114.4, 114.5, 117.5, 123.6, 129.3, 132.4, 132.5, 133.8, 141.2, 143.2, 145.0, 145.4, 152.3, 157.4 (Ar-C and C=N), 164.1 (C=O). Anal. Calcd. for  $\text{C}_{33}\text{H}_{41}\text{NO}_5$  (531.68): C, 74.55; H, 7.77; N, 2.63. Found: C, 74.46; H, 7.63; N, 2.51%.

4-(4-(Hexyloxyphenyl)iminomethyl)-3-methoxyphenyl 4-octyloxybenzoate (**I8**).

Yield: 84.0%; mp 102–104 °C, FTIR ( $\nu$ ,  $\text{cm}^{-1}$ ): 2921, 2871 ( $\text{CH}_2$  stretching), 1731 ( $\text{C}=\text{O}$ ), 1603 ( $\text{C}=\text{N}$ ), 1583 ( $\text{C}=\text{C}$ ), 1463 ( $\text{C}-\text{O}_{\text{Asym}}$ ), 1262 ( $\text{C}-\text{O}_{\text{Sym}}$ ).  $^1\text{H-NMR}$  (400 MHz,  $\text{CDCl}_3$ ):  $\delta$ /ppm: 0.86–0.91 (m, 6H,  $\text{CH}_3(\text{CH}_2)_3\text{CH}_2\text{CH}_2\text{O}-$  and  $\text{CH}_3(\text{CH}_2)_5\text{CH}_2\text{CH}_2\text{O}-$ ), 1.23–1.39 (m, 16H,  $\text{CH}_3(\text{CH}_2)_3\text{CH}_2\text{CH}_2\text{O}-$  and  $\text{CH}_3(\text{CH}_2)_5\text{CH}_2\text{CH}_2\text{O}-$ ), 1.78–1.82 (m, 4H,  $\text{CH}_3(\text{CH}_2)_3\text{CH}_2\text{CH}_2\text{O}-$  and  $\text{CH}_3(\text{CH}_2)_5\text{CH}_2\text{CH}_2\text{O}-$ ), 3.88 (s, 3H,  $\text{OCH}_3$ ), 4.01–4.05 (m, 4H,  $\text{CH}_3(\text{CH}_2)_3\text{CH}_2\text{CH}_2\text{O}-$  and  $\text{CH}_3(\text{CH}_2)_5\text{CH}_2\text{CH}_2\text{O}-$ ), 6.79–6.96 (m, 4H, Ar-H), 7.31–7.35 (d, 2H, Ar-H), 7.48–7.51 (d, 2H, Ar-H), 8.09–8.13 (m, 3H, Ar-H), 9.95 (s, 1H,  $\text{CH}=\text{N}$ ) ppm. Anal. Calcd. for  $\text{C}_{35}\text{H}_{45}\text{NO}_5$  (559.74): C, 75.10; H, 8.10; N, 2.50. Found: C, 75.25; H, 8.03; N, 2.38%.

4-(4-(Hexyloxyphenyl)iminomethyl)-3-methoxyphenyl 4-decyloxybenzoate (**I10**).

Yield: 87.5%; mp 1099–101 °C, FTIR ( $\nu$ ,  $\text{cm}^{-1}$ ): 2936, 2882 ( $\text{CH}_2$  stretching), 1728 ( $\text{C}=\text{O}$ ), 1609 ( $\text{C}=\text{N}$ ), 1575 ( $\text{C}=\text{C}$ ), 1455 ( $\text{C}-\text{O}_{\text{Asym}}$ ), 1254 ( $\text{C}-\text{O}_{\text{Sym}}$ ).  $^1\text{H-NMR}$  (400 MHz,  $\text{CDCl}_3$ ):  $\delta$ /ppm: 0.84–0.90 (m, 6H,  $\text{CH}_3(\text{CH}_2)_3\text{CH}_2\text{CH}_2\text{O}-$  and  $\text{CH}_3(\text{CH}_2)_7\text{CH}_2\text{CH}_2\text{O}-$ ), 1.23–1.45 (m, 20H,  $\text{CH}_3(\text{CH}_2)_3\text{CH}_2\text{CH}_2\text{O}-$  and  $\text{CH}_3(\text{CH}_2)_7\text{CH}_2\text{CH}_2\text{O}-$ ), 1.78–1.80 (m, 4H,  $\text{CH}_3(\text{CH}_2)_3\text{CH}_2\text{CH}_2\text{O}-$  and  $\text{CH}_3(\text{CH}_2)_7\text{CH}_2\text{CH}_2\text{O}-$ ), 3.87 (s, 3H,  $\text{OCH}_3$ ), 3.88–3.91 (t, 2H,  $\text{CH}_3(\text{CH}_2)_7\text{CH}_2\text{CH}_2\text{O}-$ ), 4.01–4.04 (t, 2H,  $\text{CH}_3(\text{CH}_2)_3\text{CH}_2\text{CH}_2\text{O}-$ ), 6.78–6.98 (m, 4H, Ar-H), 7.31–7.33 (d, 2H, Ar-H), 7.49–7.51 (d, 2H, Ar-H), 8.10–8.14 (m, 3H, Ar-H), 9.95 (s, 1H,  $\text{CH}=\text{N}$ ) ppm.  $^{13}\text{C-NMR}$  (100 MHz,  $\text{CDCl}_3$ ):  $\delta$ /ppm: 14.02 ( $\text{CH}_3$ ), 22.1, 22.6, 26.1, 28.9, 29.3, 31.2, 31.6 ( $\text{CH}_2$ ), 56.7 ( $\text{OCH}_3$ ), 68.6 ( $\text{CH}_2-\text{O}$ ), 114.5, 118.1, 121.3, 124.9, 128.1, 132.3, 133.6, 134.0, 135.9, 137.7, 140.8, 146.3 (Ar-C), 150.7 ( $\text{C}=\text{N}$ ), 152.4, 157.6 (Ar-C), 164.0 ( $\text{C}=\text{O}$ ) ppm. Anal. Calcd. for  $\text{C}_{37}\text{H}_{49}\text{NO}_5$  (587.79): C, 75.60; H, 8.40; N, 2.38. Found: C, 75.49; H, 8.31; N, 2.27%.

4-(4-(Hexyloxyphenyl)iminomethyl)-3-methoxyphenyl 4-dodecyloxybenzoate (**I12**).

Yield: 89.2%; mp 95–97 °C, FTIR ( $\nu$ ,  $\text{cm}^{-1}$ ): 2928, 2871 ( $\text{CH}_2$  stretching), 1727 ( $\text{C}=\text{O}$ ), 1610 ( $\text{C}=\text{N}$ ), 1573 ( $\text{C}=\text{C}$ ), 1462 ( $\text{C}-\text{O}_{\text{Asym}}$ ), 1464 ( $\text{C}-\text{O}_{\text{Asym}}$ ).  $^1\text{H-NMR}$  (400 MHz,  $\text{CDCl}_3$ ):  $\delta$ /ppm: 0.69–0.76 (m, 6H,  $\text{CH}_3(\text{CH}_2)_3\text{CH}_2\text{CH}_2\text{O}-$  and  $\text{CH}_3(\text{CH}_2)_9\text{CH}_2\text{CH}_2\text{O}-$ ), 1.23–1.45 (m, 24H,  $\text{CH}_3(\text{CH}_2)_3\text{CH}_2\text{CH}_2\text{O}-$  and  $\text{CH}_3(\text{CH}_2)_9\text{CH}_2\text{CH}_2\text{O}-$ ), 1.56–1.67 (m, 4H,  $\text{CH}_3(\text{CH}_2)_3\text{CH}_2\text{CH}_2\text{O}-$  and  $\text{CH}_3(\text{CH}_2)_9\text{CH}_2\text{CH}_2\text{O}-$ ), 3.72 (s, 3H,  $\text{OCH}_3$ ), 3.74–3.78 (t, 2H,  $\text{CH}_3(\text{CH}_2)_9\text{CH}_2\text{CH}_2\text{O}-$ ), 3.86–3.93 (t, 2H,  $\text{CH}_3(\text{CH}_2)_3\text{CH}_2\text{CH}_2\text{O}-$ ), 6.69–6.83 (m, 4H, Ar-H), 7.11–7.37 (m, 4H, Ar-H), 7.95–7.98 (m, 3H, Ar-H), 9.82 (s, 1H,  $\text{CH}=\text{N}$ ) ppm.  $^{13}\text{C-NMR}$  (100 MHz,  $\text{CDCl}_3$ ):  $\delta$ /ppm: 13.9 ( $2\text{CH}_3$ ), 22.1, 22.2, 25.2, 28.6, 28.9, 29.1, 29.2, 31.1, 31.5 ( $14\text{CH}_2$ ), 55.7 ( $\text{OCH}_3$ ), 67.9 ( $2\text{CH}_2-\text{O}$ ), 110.6, 113.9, 114.8, 114.9, 120.3, 123.1, 124.2, 124.3, 129.6, 132.0, 132.1, 145.0, 151.9, 157.2, 158.5 (Ar-C and  $\text{C}=\text{N}$ ), 163.5 ( $\text{C}=\text{O}$ ) ppm. Anal. Calcd. for  $\text{C}_{39}\text{H}_{53}\text{NO}_5$  (615.84): C, 76.06; H, 8.67; N, 2.27. Found: C, 76.00; H, 8.57; N, 2.14%.

4-(4-(Hexyloxyphenyl)iminomethyl)-3-methoxyphenyl 4-hexadecyloxybenzoate (**I16**).

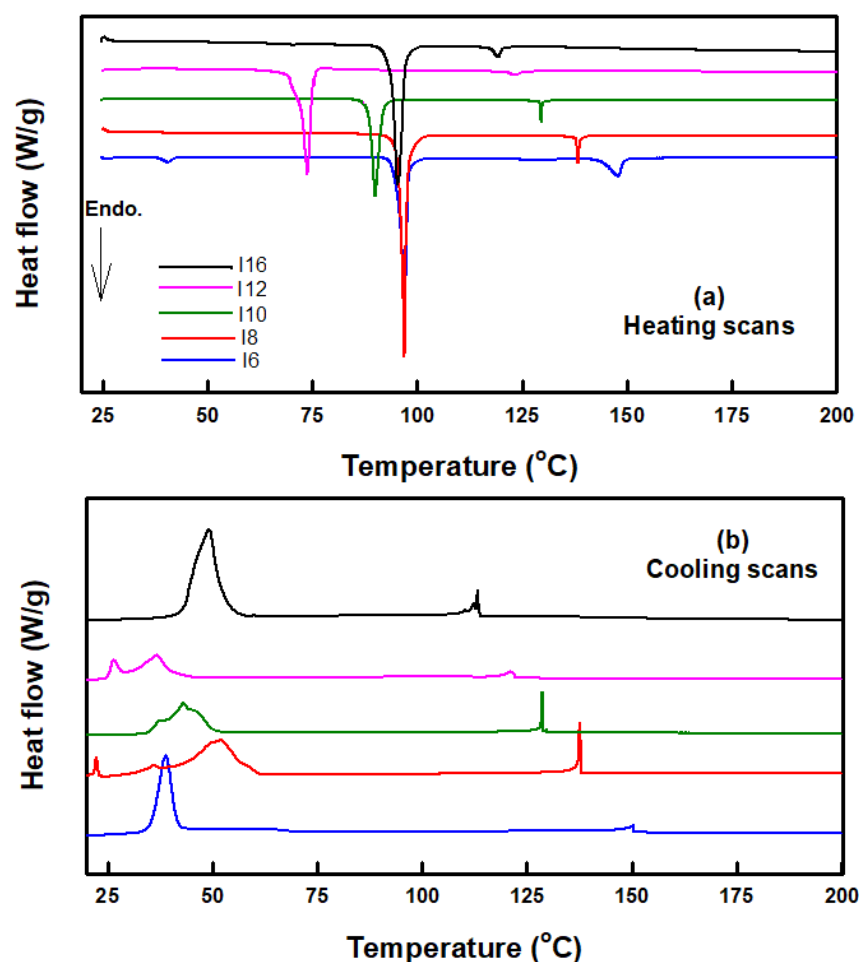
Yield: 90.1%; mp 90–92 °C, FTIR ( $\nu$ ,  $\text{cm}^{-1}$ ): 2923, 2882 ( $\text{CH}_2$  stretching), 1729 ( $\text{C}=\text{O}$ ), 1612 ( $\text{C}=\text{N}$ ), 1580 ( $\text{C}=\text{C}$ ), 1464 ( $\text{C}-\text{O}_{\text{Asym}}$ ), 1251 ( $\text{C}-\text{O}_{\text{Sym}}$ ).  $^1\text{H-NMR}$  (400 MHz,  $\text{CDCl}_3$ ):  $\delta$ /ppm: 0.84–0.90 (m, 6H,  $\text{CH}_3(\text{CH}_2)_3\text{CH}_2\text{CH}_2\text{O}-$  and  $\text{CH}_3(\text{CH}_2)_7\text{CH}_2\text{CH}_2\text{O}-$ ), 1.24–1.43 (m, 32H,  $\text{CH}_3(\text{CH}_2)_3\text{CH}_2\text{CH}_2\text{O}-$  and  $\text{CH}_3(\text{CH}_2)_7\text{CH}_2\text{CH}_2\text{O}-$ ), 1.71–1.84 (m, 4H,  $-\text{CH}_3(\text{CH}_2)_3\text{CH}_2\text{CH}_2\text{O}-$  and  $\text{CH}_3(\text{CH}_2)_7\text{CH}_2\text{CH}_2\text{O}-$ ), 3.87 (s, 3H,  $\text{OCH}_3$ ), 3.88–3.90 (t, 2H,  $\text{CH}_3(\text{CH}_2)_7\text{CH}_2\text{CH}_2\text{O}-$ ), 4.00–4.03 (t, 2H,  $\text{CH}_3(\text{CH}_2)_3\text{CH}_2\text{CH}_2\text{O}-$ ), 6.94–6.97 (m, 4H, Ar-H), 7.30–7.32 (d, 2H, Ar-H), 7.49–7.51 (d, 2H, Ar-H), 8.11–8.14 (m, 3H, Ar-H), 9.95 (s, 1H,  $\text{CH}=\text{N}$ ) ppm. Anal. Calcd. for  $\text{C}_{43}\text{H}_{61}\text{NO}_5$  (671.95): C, 76.86; H, 9.15; N, 2.08. Found: C, 76.93; H, 9.01; N, 1.95%.

### 3. Results and Discussion

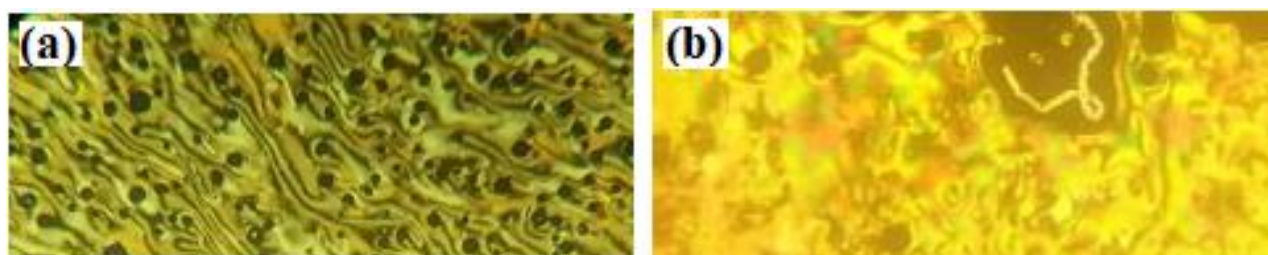
#### 3.1. Optical and Mesophase Studies

The mesomorphic and optical characterizations for the synthesized laterally methoxy-substituted homologous, **In**, were investigated by differential scanning calorimetry (DSC) and their textures identified by polarized optical microscopy (POM). DSC thermograms of designed compounds (**In**), through heating and cooling cycles, are shown in Figure 2. It is clearly shown that upon heating, all compounds (Figure 2a) showed two endotherms intrinsic peaks ascribed to the crystal-to-nematic and nematic-to-isotropic liquid transitions. During the cooling cycle, all derivatives were shown to possess only the nematic mesophase

(Figure 2b). The POM investigations revealed images which confirm the threads/schlieren nematic mesophase (Figure 3). This means that these materials exhibited the monomorphic enantiotropic property. Transition temperatures, enthalpies, normalized entropies and the nematic temperature ranges, recorded by DSC measurements upon heating, were collected in Table 1. Figure 4 depicts the graphical plot of the transition temperatures of all designed compounds in order to evaluate the effect of the terminal alkoxy chain length ( $n$ ) on the mesomorphic and optical behaviors of the prepared series, **I $n$** .



**Figure 2.** The recorded DSC thermograms of series **I $n$**  at a rate of  $\pm 10$  °C/min (a) the second heating and (b) cooling scans.

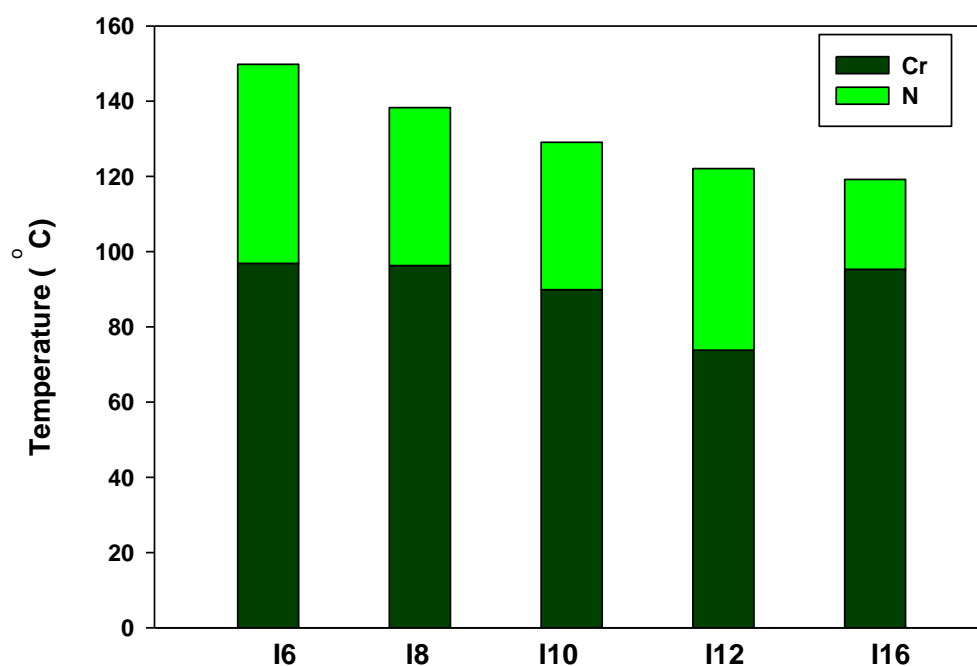


**Figure 3.** Textures observed upon heating under POM of nematic mesophase for (a) compound **I6** at 141.0 °C and (b) compound **I16** at 116.0 °C.

**Table 1.** Mesophase transition temperatures ( $^{\circ}\text{C}$ ), enthalpy  $\Delta H$ , kJ/mole, and normalized entropy of transition  $\Delta S/R$  for compounds **I***n*.

Comp.	$T_{\text{Cr-N}}$	$\Delta H_{\text{Cr-N}}$	$T_{\text{N-I}}$	$\Delta H_{\text{N-I}}$	$\Delta T_{\text{N}}$	$\Delta S_{\text{N-I}}/R$
<b>I6</b>	96.9	44.9	149.8	1.5	52.9	0.4
<b>I8</b>	96.3	51.5	138.3	2.8	42.0	0.8
<b>I10</b>	89.9	49.3	129.1	2.2	39.2	0.7
<b>I12</b>	73.8	44.3	122.1	1.0	48.3	0.3
<b>I16</b>	95.3	54.7	119.2	3.0	23.9	0.9

Cr-N = solid to the nematic phase; N-I = nematic to the isotropic liquid phase.

**Figure 4.** Impact of terminal chain length (*n*) on the mesomorphic behavior of the present homologous **I***n* series.

Data illustrated in Table 1 and Figure 4 indicate that the melting transitions ( $T_{\text{Cr-N}}$ ) of all of the prepared homologues, independent of the length of the terminal chain, exhibit irregular trends. In general, the melting point is related with the polarizability of the compound as well as the packing of crystalline molecules and other factors. Data also show that all the members of the homologous series are enantiotropic with suitable nematic thermal stability and nematic temperature range. As usual, the stability of the N mesophase decreased with increases to the length of terminal chain (*n*), [40,41]. That descending trend of the nematic thermal stability with the increase of the flexible-chain length is ascribed to the dilution of the rigid mesogenic core.  $T_{\text{N-I}}$  transitions were showed to decrease from 149.8 to 119.2  $^{\circ}\text{C}$  as *n* increased from 6 to 16 carbons. Moreover, the homologue with the shortest chain (**I6**) exhibited the highest N temperature range ( $\Delta T_{\text{N}} = 52.9^{\circ}\text{C}$ ), while the N phase range for the longest chain (**I16**) showed the lowest value ( $\Delta T_{\text{N}} = 23.9^{\circ}\text{C}$ ). The decline of  $\Delta T_{\text{N}}$  is not regular but obeys the order of **I6** > **I12** > **I8** > **I10** > **I16**. It was known that the rigidity, aspect ratio, molecular geometry, polarity and polarizability of the molecule were considered essential factors that are responsible for the thermal stability of the observed mesophases. The different contribution extents of these factors lead to differences in the mesophase property. Generally, the thermal stability of a phase of a given liquid crystalline material is increased by influences of the polarity or polarizability of the molecule mesogenic core that is actually affected by the polarity of the attached group, which would consequently affect the polarity of the whole molecule. Furthermore, the

kind and stability of the formed phase are mainly dependent upon the dipole moment of the mesogenic group of the molecule which differs according to the position of the polar substituent too [42].

The normalized transition entropy changes,  $\Delta S_{N-I}/R$ , of the synthesized lateral methoxy derivatives (**I $n$** ) are collected in Table 1. The results revealed that the value of the entropy change was related, independently, to the length of the terminal chains ( $n$ ). The small values observed for the entropy change can be attributed to the decrease of the length-to-breadth ratio resulting from their lower anisotropy in terms of their molecular geometry and the increment of their molecular biaxiality [42,43]. Moreover, due to the nematic nature of the mesophase, this exhibits the lowest order mesophase.

### 3.2. Thermal Properties Studies

Thermal stability of the present homologous set (**I $n$** ) was measured by thermogravimetric analysis (TG). A representative example of TG curve, and its corresponding derivative (DTG) of the compounds **I6**, is depicted in Figure 5. Parameters of thermal degradation, such as  $T_{\text{onset}}$  (the start thermal degradation temperature),  $T_{\text{max}}$  (the temperature at which the thermal degradation rate is maximum), and  $m\%$  (the mass percentage loss), were estimated. As can be seen from Figure 5, the decomposition occurs through two degradation steps (the second step is not seen in (DTG)) depending on the molecular structure. The first step occurs in the temperature range of  $\approx 250\text{--}300\text{ }^{\circ}\text{C}$  and starts at  $280\text{ }^{\circ}\text{C}$  with the maximum degradation rate ( $T_{\text{max}}$ ) at  $300\text{ }^{\circ}\text{C}$ , indicating that the material has high thermal stability. The second step occurs between  $330$  and  $400\text{ }^{\circ}\text{C}$ , with the maximum degradation rate of  $\approx 350\text{ }^{\circ}\text{C}$ . For all prepared homologues series, the first main step occurs with maximum degradation rates ( $T_{\text{max}}$ ) at  $350, 353, 358, 361$  and  $368\text{ }^{\circ}\text{C}$  for **I6, I8, I10, I12** and **I16**, respectively, indicating that the thermal stability of materials increases with  $n$  (See Figures S1–S4 in supplementary data). Results revealed that the investigated compounds exhibited high thermal stabilities up to  $350\text{--}368\text{ }^{\circ}\text{C}$ , which covers the temperature window of mesophase transition detected thermally and extends over this transition too.

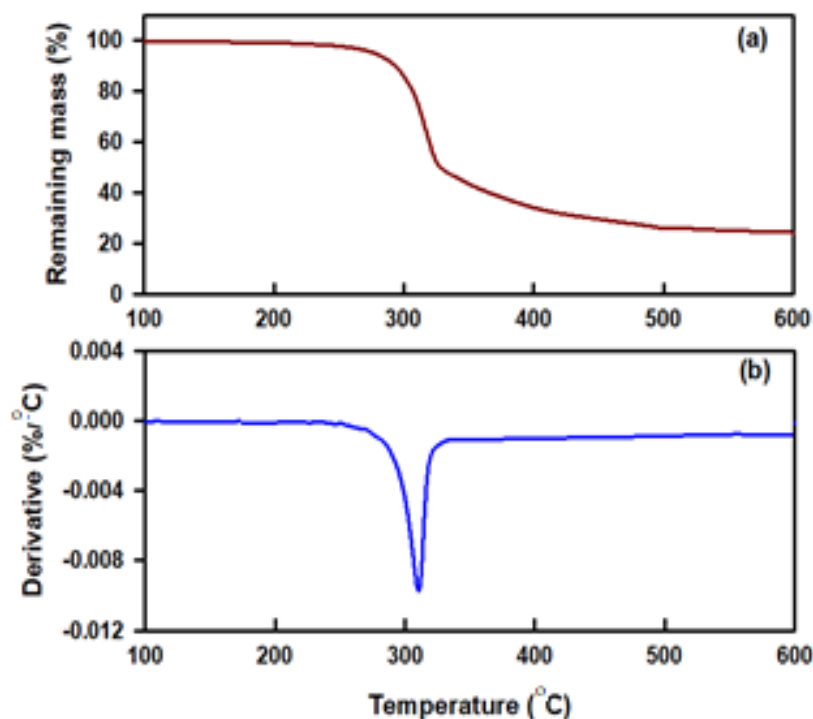


Figure 5. TG (a) and DTG (b) curves of the compound **I6**.

### 3.3. Effect of the Lateral Methoxy Group on the Mesomorphic Behaviors

Because of its small size, the incorporation of the lateral methoxy group into the mesogenic part of the molecule was accompanied by a slight steric effect. Moreover, since this is an electron donating group, it affected the intermolecular dispersion interactions. In order to analyze the effect of the special orientation and location of the lateral  $\text{OCH}_3$  group in the middle ring of the molecule on the mesomorphic and thermal stability of the compounds, a comparison was established between the present synthesized lateral methoxy derivatives (**I***n*) and the previously documented laterally neat homologues series **II***n* [44]; graphically represented in Figure 6a for the mesomorphic stability, and their temperature ranges in Figure 6b. As can be seen from Figure 6a, the type and thermal stability of the formed mesophase varied according to the impacted molecular dipole moment and polarizability of the mesogenic moiety, which were dependent upon the orientation and position of the lateral methoxy group. Moreover, the addition of the lateral  $\text{OCH}_3$  group into the ortho-position with respect to the azomethine linkage of **I***n*, was shown to disrupt the smectic A molecular packing and give only N mesophase. The mesomeric interactions of the lateral methoxy group with the carbonyl ester  $\text{C}=\text{O}$  moiety may be prohibited to the extent that the present compounds (**I***n*) possess lower thermal stability than the laterally neat homologue (**II***n*). The mesophase thermal stability was dependent on the enhanced dipole of the mesogenic portion of the molecule, which was mainly dependent on the position of the lateral  $\text{OCH}_3$  group. In addition to the molecular geometry of the molecule, which varied according to the location of the attached substituent, it also had high effects on the molecular thermal stability. For the nematic range (Figure 6b) the laterally neat series, **II***n*, showed higher N temperature ranges than the laterally methoxy-substituted analogues, **I***n*, in the short terminal chain lengths ( $n = 6, 8$ ), while for longer terminals ( $n \geq 10$ ) the present laterally substituted series showed wider N temperature ranges than the previously investigated laterally neat analogues. The comparison revealed that the mesophase type and stability, as well as the temperature range, depended on the protrusion of the lateral  $\text{OCH}_3$  group, which was incorporated within the mesogenic portion of the molecule. Furthermore, it was found that the introducing of the methoxy group into the  $\pi$ -system induced a bathochromic shift in the absorption spectrum of the molecule and improved the light absorption characteristics [45].

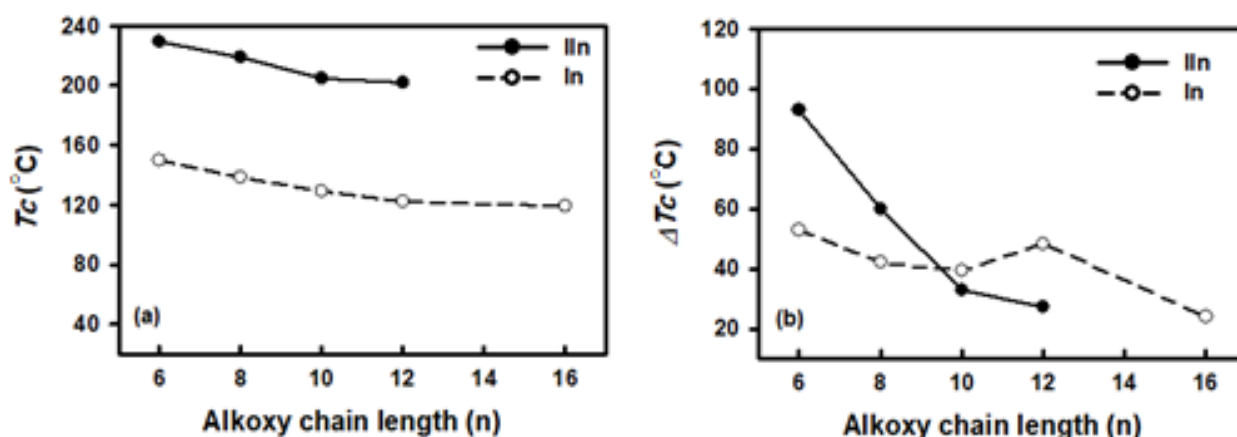


Figure 6. Comparison of (a)  $T_c$  and (b)  $\Delta T_c$  of homologues series **I***n* and **II***n*.

### 3.4. Photoactive Studies

UV-vis absorption spectra were measured for the present lateral methoxy-substituted derivatives (**I***n*) in dichloromethane solution ( $C = 1.1 \times 10^{-3} \text{ mol L}^{-1}$ ) and the results are represented graphically in Figure 7. As can be seen from Figure 7, the length of terminal alkoxy chain enhanced the maximum absorbance of the members of homologous series, **I***n*. Figure 7 also showed that the absorption of light within the wavelength range 380–800 nm, and its strong absorption maxima at ~442–453 nm due to the terminal alkoxy

carbon chain ( $n$ ), can be attributed to the  $\pi$ - $\pi^*$  transition of the chromophore within the molecule. Moreover, the intensity of the peak and absorption bands is dependent on the geometry of the molecule that absorbs the light at a given wavelength. The absorption spectra of I16 showed the maximum bands at 453 nm, which is also due to the  $\pi$ - $\pi$  electronic transitions from the highest occupied molecular orbitals (HOMO) to the lowest unoccupied molecular orbitals (LUMO) [46–49]. The present nematogenic materials are promising for use in photoactive organic compounds for many applications.

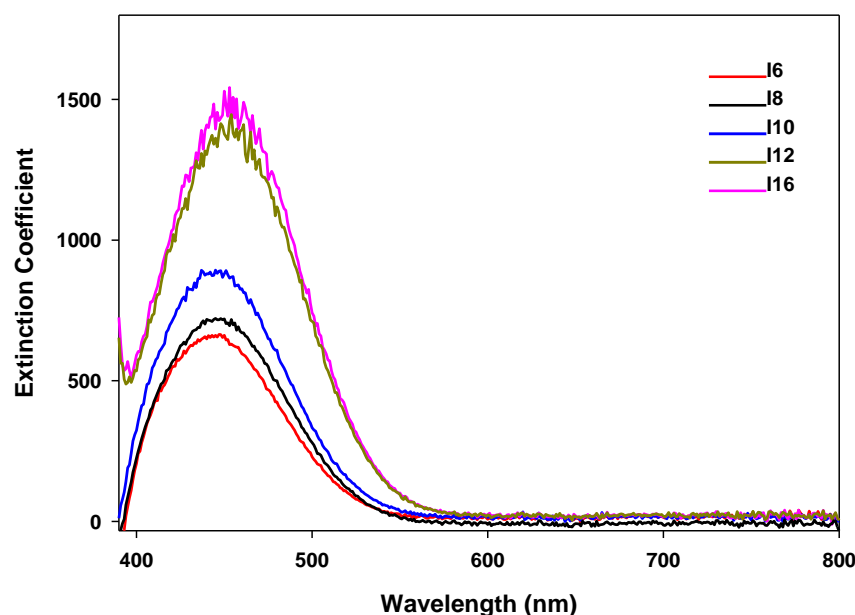


Figure 7. UV-vis spectra of present series,  $I_n$ , in  $\text{CH}_2\text{Cl}_2$  at 25 °C.

#### 4. Conclusions

We have documented the synthesis of new optical lateral-methoxy Schiff base/ester homologues using different thermal, optical and mesomorphic techniques. Molecular structures were elucidated by FT-IR and NMR spectroscopy. Mesomorphic, optical and thermal behaviors were characterized using DSC, POM, TGA as well as UV-vis spectroscopy. Results revealed that all members of the homologues series exhibited only the monomorphic N phase irrespective of the terminal alkoxy-chain length. On the other hand, their thermal stabilities were shown to be dependent on the length of the terminal chain. A comparative study was made between the present group of homologues and their corresponding laterally-neat Schiff base/ester analogues. The study revealed that the type and thermal mesophase stability were influenced by the incorporated lateral  $\text{OCH}_3$  group within the mesogenic portion of the molecule. Finally, the proper choice for new optical organic materials, which possess nematic temperature range, good thermal stability and are affected by UV-light, are promising additional factors for industrial applications.

**Supplementary Materials:** The following are available online at <https://www.mdpi.com/article/10.3390/cryst11050551/s1>. Figure S1: TG (a) and DTG (b) curves of the compound I8. Figure S2: TG (a) and DTG (b) curves of the compound I10. Figure S3: TG (a) and DTG (b) curves of the compound I12. Figure S4: TG (a) and DTG (b) curves of the compound I16.

**Author Contributions:** Conceptualization, L.A.A.-M. and H.A.A.; methodology, L.A.A.-M., L.A.A. and H.A.A.; validation, L.A.A.-M., L.A.A. and S.M.G.; formal analysis, L.A.A.-M. and H.A.A.; investigation, L.A.A.-M. and H.A.A.; resources, L.A.A. and S.M.G.; data curation, H.A.A.; writing—original draft preparation, H.A.A., L.A.A.-M. and S.M.G.; writing—review and editing, L.A.A.-M., L.A.A., H.A.A., S.M.G.; visualization, H.A.A.; supervision, L.A.A.-M. and H.A.A.; project administration, L.A.A.-M. and L.A.A.; funding acquisition, L.A.A.-M. All authors have read and agreed to the published version of the manuscript.

**Funding:** This research project was funded by the Deanship of Scientific Research, Princess Nourah bint Abdulrahman University, through the Program of Research Project Funding After Publication, grant No (PRFA-P-42-8).

**Data Availability Statement:** The data presented in this study are available on request from the corresponding author.

**Acknowledgments:** This research project was funded by the Deanship of Scientific Research, Princess Nourah bint Abdulrahman University, through the Program of Research Project Funding After Publication, grant No (PRFA-P-42-8).

**Conflicts of Interest:** The authors declare no conflict of interest.

## References

1. Kelker, H.; Scheurle, B. A Liquid-crystalline(Nematic) Phase with a Particularly Low Solidification Point. *Angew. Chem. Int. Ed.* **1969**, *8*, 884–885. [\[CrossRef\]](#)
2. Kato, T.; Uchida, J.; Ichikawa, T.; Sakamoto, T. Functional Liquid Crystals towards the Next Generation of Materials. *Angew. Chem. Int. Ed.* **2018**, *57*, 4355–4371. [\[CrossRef\]](#)
3. Sharma, V.S.; Patel, R.B. Design and investigation of calamatic liquid crystals: Schiff base (-CH=N), chalcone (-CO-CH=CH-), and ester (-COO-) linkage group contain rigid rod shape with various terminal parts. *Mol. Cryst. Liq. Cryst.* **2017**, *643*, 141–158. [\[CrossRef\]](#)
4. Ahmed, N.H.S.; Saad, G.R.; Ahmed, H.A.; Hagar, M. New wide-stability four-ring azo/ester/Schiff base liquid crystals: Synthesis, mesomorphic, photophysical, and DFT approaches. *RSC Adv.* **2020**, *10*, 9643–9656. [\[CrossRef\]](#)
5. Al-Mutabagani, L.; Alshabanah, L.A.; Ahmed, H.; Abu Al-Ola, K.; Hagar, M. New Rod-like H-bonded Assembly Systems: Mesomorphic and Geometrical Aspects. *Crystals* **2020**, *10*, 795. [\[CrossRef\]](#)
6. Ahmed, H.A.; Hagar, M.; Aljuhani, A. Mesophase behavior of new linear supramolecular hydrogen-bonding complexes. *RSC Adv.* **2018**, *8*, 34937–34946. [\[CrossRef\]](#)
7. Ahmed, H.A.; Mansour, E.; Hagar, M. Mesomorphic study and DFT simulation of calamitic Schiff base liquid crystals with electronically different terminal groups and their binary mixtures. *Liq. Cryst.* **2020**, *47*, 2292–2304. [\[CrossRef\]](#)
8. Kelker, H.; Scheurle, B. Eine flüssig-kristalline (nematische) Phase mit besonders niedrigem Erstarrungspunkt. *Angew. Chem.* **1969**, *81*, 903–904. [\[CrossRef\]](#)
9. Saccone, M.; Kuntze, K.; Ahmed, Z.; Siiskonen, A.; Giese, M.; Priimagi, A. ortho-Fluorination of azophenols increases the mesophase stability of photoresponsive hydrogen-bonded liquid crystals. *J. Mater. Chem. C* **2018**, *6*, 9958–9963. [\[CrossRef\]](#)
10. Jessy, P.; Radha, S.; Patel, N. Morphological, optical and dielectric behavior of chiral nematic liquid crystal mixture: Study on effect of different amount of chirality. *J. Mol. Liq.* **2018**, *255*, 215–223. [\[CrossRef\]](#)
11. Mishra, R.; Hazarika, J.; Hazarika, A.; Gogoi, B.; Dubey, R.; Bhattacharjee, D.; Singh, K.N.; Alapati, P.R. Dielectric properties of a strongly polar nematic liquid crystal compound doped with gold nanoparticles. *Liq. Cryst.* **2018**, *45*, 1661–1671. [\[CrossRef\]](#)
12. Zaki, A.A. Optical measurements of phase transitions in difluorophenylazophenyl benzoate thermotropic liquid crystal with specific orientated fluorine atoms. *Phase Transit.* **2018**, *92*, 135–148. [\[CrossRef\]](#)
13. Zaki, A.A.; Ahmed, H.; Hagar, M. Impact of fluorine orientation on the optical properties of difluorophenylazophenyl benzoates liquid crystal. *Mater. Chem. Phys.* **2018**, *216*, 316–324. [\[CrossRef\]](#)
14. Naoum, M.M.; Saad, G.R.; Nessim, R.I.; Abdel-Aziz, T.A.; Seliger, H. Effect of molecular structure on the phase behaviour of some liquid crystalline compounds and their binary mixtures II. 4-Hexadecyloxyphenyl arylates and aryl 4-hexadecyloxy benzoates. *Liq. Cryst.* **1997**, *23*, 789–795. [\[CrossRef\]](#)
15. Saad, G.R.; Nessim, R.I. Effect of molecular structure on the phase behaviour of some liquid crystalline compounds and their binary mixtures VI[1]. The effect of molecular length. *Liq. Cryst.* **1999**, *26*, 629–636. [\[CrossRef\]](#)
16. Naoum, M.; Ş, S.M.; Ahmed, H. Lateral protrusion and mesophase behaviour in pure and mixed states of model compounds of the type 4-(4'-substituted phenylazo)-2-(or 3-)methyl phenyl-4'-alkoxy benzoates. *Liq. Cryst.* **2010**, *37*, 1245–1257. [\[CrossRef\]](#)
17. Luckhurst, G.; Gray, G.W. *The molecular Physics of Liquid Crystals*; Academic Press: Cambridge, MA, USA, 1979.
18. Ahmed, H.A.; El-Atawy, M.A. Synthesis, mesomorphic and geometrical approaches of new non-symmetrical system based on central naphthalene moiety. *Liq. Cryst.* **2021**. [\[CrossRef\]](#)
19. El-Atawy, M.A.; Naoum, M.M.; Al-Zahrani, S.A.; Ahmed, H.A. New Nitro-Laterally Substituted Azomethine Derivatives; Synthesis, Mesomorphic and Computational Characterizations. *Molecules* **2021**, *26*, 1927. [\[CrossRef\]](#)
20. Takezoe, H.; Takanishi, Y. Bent-Core Liquid Crystals: Their Mysterious and Attractive World. *Jpn. J. Appl. Phys.* **2006**, *45*, 597–625. [\[CrossRef\]](#)
21. Ahmed, H.A.; Hagar, M.; El-Sayed, T.H.; Alnoman, R.B. Schiff base/ester liquid crystals with different lateral substituents: Mesophase behaviour and DFT calculations. *Liq. Cryst.* **2019**, *46*, 1–11. [\[CrossRef\]](#)
22. Naveen, K.; Udayabhanu, A.; Mahadevan, K.M.; Nagaraju, G. Solvent free and green synthesis of efficient solvochromism based coumarin moieties for quick visualization of LFPs and OLEDs applications. *J. Mol. Struct.* **2021**, *1223*, 129208.

23. Ghasem, B.; Shahram, M.; Saeed, S. A novel method for the synthesis of coumarin laser dyes derived from 3-(1H-benzimidazol-2-yl) coumarin-2-one under microwave irradiation. *Arab. J. Chem.* **2014**, *7*, 972.
24. Aulsebrook, M.L.; Graham, B.; Grace, M.R.; Tuck, K.L. Coumarin-based fluorescent sensors for zinc (II) and hypo-chlorite. *Supramol. Chem.* **2015**, *27*, 798. [[CrossRef](#)]
25. Huang, X.; Dong, Y.; Huang, Q.; Cheng, Y. Hydrogen bond induced fluorescence recovery of coumarin-based sensor system. *Tetrahedron Lett.* **2013**, *54*, 3822–3825. [[CrossRef](#)]
26. Khan, R.I.; Pitchumani, K. beta-Cyclodextrin included coumarin derivatives as selective fluorescent sensors for Cu<sup>2+</sup> ions in HeLa cells. *Royal Soc. Chem. Adv.* **2016**, *6*, 20269.
27. Breul, A.M.; Hager, M.D.; Schubert, U.S. Fluorescent monomers as building blocks for dye labeled polymers: Synthesis and application in energy conversion, biolabeling and sensors. *Chem. Soc. Rev.* **2013**, *42*, 5366–5407. [[CrossRef](#)] [[PubMed](#)]
28. Zhang, X.; Feng, H.; Yan, M.; Guo, H.; Yang, F. The novel rufigallol-based liquid crystals with cholesterol units: Synthesis, mesomorphic and photophysical properties. *Liq. Cryst.* **2019**, *46*, 787–796. [[CrossRef](#)]
29. Lin, L.; Qin, W.; Cheng, B.; Guo, H.; Yang, F. The influence of multiple alkyl chains on mesomorphic and photophysical properties of diphenylacrylonitrile liquid crystals. *Liq. Cryst.* **2019**, *47*, 967–976. [[CrossRef](#)]
30. Young-Ki, K.; Bohdan, S.; Oleg, D. Lavrentovich. Molecular reorientation of a nematic liquid crystal by thermal expansion. *Nat. Commun.* **2012**, *3*, 1113.
31. Sayed, R.; Abd El-lateef, H.M.; Gomha, S.M. L-Proline catalyzed green synthesis and anticancer evaluation of novel bi-oactive benzil bis-hydrazones under grinding technique. *Green Chem. Lett. Rev.* **2021**, *14*, 179–188. [[CrossRef](#)]
32. Gomha, S.M.; A Abdelhady, H.; Hassain, D.Z.; Abdelmonsef, A.H.; El-Naggar, M.; Elaasser, M.M.; Mahmoud, H.K. Thiazole-Based Thiosemicarbazones: Synthesis, Cytotoxicity Evaluation and Molecular Docking Study. *Drug Des. Dev. Ther.* **2021**, *ume 15*, 659–677. [[CrossRef](#)]
33. Gomha, S.M.; Muhammad, Z.A.; Abdel-Aziz, H.M.; Matar, I.K.; El-Sayed, A.A. Green synthesis, molecular docking and anticancer activity of novel 1,4-dihydropyridine-3,5-Dicarbohydrazones under grind-stone chemistry. *Green Chem. Lett. Rev.* **2020**, *13*, 6–17. [[CrossRef](#)]
34. Gomha, S.M.; Edrees, M.M.; Muhammad, Z.A.; Kheder, N.A.; Melha, S.A.-; Saad, A.M. Synthesis, Characterization, and Antimicrobial Evaluation of Some New 1,4-Dihydropyridines-1,2,4-Triazole Hybrid Compounds. *Polycycl. Aromat. Compd.* **2020**, 1–13. [[CrossRef](#)]
35. Gomha, S.M.; Riyadh, S.M. Synthesis under Microwave Irradiation of [1,2,4]Triazolo[3,4-b] [1,3,4]thiadiazoles and Other Diazoles Bearing Indole Moieties and Their Antimicrobial Evaluation. *Molecules* **2011**, *16*, 8244–8256. [[CrossRef](#)] [[PubMed](#)]
36. Abu-Melha, S.; Edrees, M.M.; Riyadh, S.M.; Abdelaziz, M.R.; Elfiky, A.A.; Gomha, S.M. Clean grinding technique: A facile synthesis and in silico antiviral activity of hydrazones, pyrazoles, and pyrazines bearing thiazole moiety against SARS-CoV-2 main protease (Mpro). *Molecules* **2020**, *25*, 4565. [[CrossRef](#)] [[PubMed](#)]
37. Sayed, A.R.; Gomha, S.M.; A Taher, E.; A Muhammad, Z.; El-Seedi, H.R.; Gaber, H.M.; Ahmed, M.M. One-Pot Synthesis of Novel Thiazoles as Potential Anti-Cancer Agents. *Drug Des. Dev. Ther.* **2020**, *ume 14*, 1363–1375. [[CrossRef](#)]
38. Ouf, S.A.; Gomha, S.M.; Ewies, M.M.; Ouf, A.S.; Sharawy, I.A.A. Antidermatophytic activity of some newly synthe-sized arylhydrazonothiazoles conjugated with monoclonal antibody. *Sci. Rep.* **2020**, *10*, 20863. [[CrossRef](#)]
39. Rashdan, H.R.M.; Abdelmonsef, A.H.; Shehadi, I.A.; Gomha, S.M.; Soliman, A.M.M.; Mahmoud, H.K. Synthesis, molecular docking screening and anti-proliferative potency evaluation of some new imidazo[2,1-b]thiazole linked thiadiazole conjugates. *Molecules* **2020**, *25*, 4997. [[CrossRef](#)] [[PubMed](#)]
40. Imrie, C.T.; Taylor, L. The preparation and properties of low molar mass liquid crystals possessing lateral alkyl chains. *Liq. Cryst.* **1989**, *6*, 1–10. [[CrossRef](#)]
41. Imrie, C.T. Non-symmetric liquid crystal dimers: How to make molecules intercalate. *Liq. Cryst.* **2006**, *33*, 1449–1485. [[CrossRef](#)]
42. Attard, G.; Imrie, C.; Karasz, F. Low molar mass liquid crystalline glasses: Preparation and properties of the. al-pi-(4-cyanobiphenyl-4'-oxy)-. omega-(1-pyrenimin ebenzylidene-4'-oxy) alkanes. *Chem. Mater.* **1992**, *4*, 1246–1253. [[CrossRef](#)]
43. Attard, G.S.; Imrie, C.T. Liquid-crystalline and glass-forming dimers derived from 1-aminopyrene. *Liq. Cryst.* **1992**, *11*, 785–789. [[CrossRef](#)]
44. Ahmed, H.A.; Hagar, M.; Saad, G.R. Impact of the proportionation of dialkoxy chain length on the mesophase behaviour of Schiff base/ester liquid crystals; experimental and theoretical study. *Liq. Cryst.* **2019**, *46*, 1611–1620. [[CrossRef](#)]
45. Avhad, K.; Jadhav, M.; Patil, D.; Chowdhury, T.H.; Islam, A.; Bedja, I.; Sekar, N. Rhodanine-3-acetic acid containing D-pi-A push-pull chromophores: Effect of methoxy group on the performance of dye-sensitized solar cells. *Org. Electron.* **2019**, *65*, 386–393. [[CrossRef](#)]
46. Yang, M.; Liu, Z.; Li, X.; Yuan, Y.; Zhang, H. Influence of flexible spacer length on self-organization behaviors and photophysical properties of hemiphasmidic liquid crystalline polymers containing cyanostilbene. *Eur. Polym. J.* **2020**, *123*, 109459. [[CrossRef](#)]
47. Ahmed, H.A.; Khushaim, M.S. Nematic Phase Induced from Symmetrical Supramolecular H-Bonded Systems Based on Flexible Acid Core. *Cryst.* **2020**, *10*, 801. [[CrossRef](#)]
48. Ahmed, H.; Khushaim, M.S. Nematogenic Laterally Substituted Supramolecular H-Bonded Complexes Based on Flexible Core. *Cryst.* **2020**, *10*, 878. [[CrossRef](#)]
49. Al-Mutabagani, L.A.; Alshabanah, L.A.; Naoum, M.M.; Hagar, M.; Ahmed, H.A. Experimental and Computational Approaches of Newly Polymorphic Supramolecular H-Bonded Liquid Crystal Complexes. *Front. Chem.* **2020**, *8*, 930. [[CrossRef](#)]